USGS
science for a changing world

Prepared in cooperation with the Bureau of Land Management

# Color Shaded-Relief and Surface-Classification Maps of the Fish Creek Area, Harrison Bay Quadrangle, Northern Alaska

By John C. Mars, Christopher P. Garrity, David W. Houseknecht,
Lee Amoroso, and Donald C. Meares

*Explanatory text to accompany*
Scientific Investigations Map 2948

2007

U.S. Department of the Interior
U.S. Geological Survey

**U.S. Department of the Interior**
DIRK KEMPTHORNE, Secretary

**U.S. Geological Survey**
Mark D. Myers, Director

U.S. Geological Survey, Reston, Virginia: 2007

For product and ordering information:
World Wide Web: http://www.usgs.gov/pubprod
Telephone: 1-888-ASK-USGS

For more information on the USGS—the Federal source for science about the Earth, its natural and living resources, natural hazards, and the environment:
World Wide Web: http://www.usgs.gov
Telephone: 1-888-ASK-USGS



Suggested citation:
Mars, J.C., Garrity, C.P., Houseknecht, D.W., Amoroso, Lee, and Meares, D.C., 2007, Color shaded-relief and surface-classification maps of the Fish Creek area, Harrison Bay quadrangle, northern Alaska: U.S. Geological Survey Scientific Investigations Map 2948, available only online at http://pubs.usgs.gov/sim/2007/2948/.

# Contents



# Figures

# Sheets

1. Color shaded-relief map
2. Surface-classification map
3. Combined shaded-relief and surface-classification map

# Color Shaded-Relief and Surface-Classification Maps of the Fish Creek Area, Harrison Bay Quadrangle, Northern Alaska

By John C. Mars,[1] Christopher P. Garrity,[1] David W. Houseknecht,[1]
Lee Amoroso,[2] and Donald C. Meares[3]

## Introduction

The northeastern part of the National Petroleum Reserve in Alaska (NPRA) has become an area of active petroleum exploration during the past five years. Recent leasing and exploration drilling in the NPRA requires the U.S. Bureau of Land Management (BLM) to manage and monitor a variety of surface activities that include seismic surveying, exploration drilling, oil-field development drilling, construction of oil-production facilities, and construction of pipelines and access roads. BLM evaluates a variety of permit applications, environmental impact studies, and other documents that require rapid compilation and analysis of data pertaining to surface and subsurface geology, hydrology, and biology. In addition, BLM must monitor these activities and assess their impacts on the natural environment. Timely and accurate completion of these land-management tasks requires elevation, hydrologic, geologic, petroleum-activity, and cadastral data, all integrated in digital formats at a higher resolution than is currently available in nondigital (paper) formats.

To support these land-management tasks, a series of maps was generated from remotely sensed data in an area of high petroleum-industry activity (fig. 1). The maps cover an area from approximately latitude 70°00' N. to 70°30' N. and from longitude 151°00' W. to 153°10' W. The area includes the Alpine oil field in the east, the Husky Inigok exploration well (site of a landing strip) in the west, many of the exploration wells drilled in NPRA since 2000, and the route of a proposed pipeline to carry oil from discovery wells in NPRA to the Alpine oil field. This map area is referred to as the "Fish Creek area" after a creek that flows through the region.

The map series includes (1) a color shaded-relief map based on 5-m-resolution data (sheet 1), (2) a surface- classification map based on 30-m-resolution data (sheet 2), and (3) a 5-m-resolution shaded relief-surface classification map that combines the shaded-relief and surface-classification data (sheet 3). Remote sensing datasets that were used to compile the maps include Landsat 7 Enhanced Thematic Mapper+ (ETM+), and interferometric synthetic aperture radar (IFSAR) data. In addition, a 1:250,000-scale geologic map of the Harrison Bay quadrangle, Alaska (Carter and Galloway, 1985, 2005) was used in conjunction with ETM+ and IFSAR data.

## Data and Methods

### Landsat 7 ETM+ Data

The Landsat 7 ETM+ radiance-at-the-sensor data were acquired on June 6, 2003, and consist of (1) six bands at 30 m resolution in the 0.4 to 2.5 micrometer (μm) region, (2) one band at 90 m resolution centered at 11.45 μm, and (3) one panchromatic band at 15 m resolution. The thermal-infrared and panchromatic bands were not used in this study. The Landsat 7 ETM+ scene was calibrated to reflectance using an ENVI (Environment for Visualizing Images) reflectance algorithm (Research Systems Incorporated, 2000). Evaluation of the reflectance data indicated that values in bands 1 through 4 were anomalously high; therefore, a dark-object subtracton method (Crain, 1971) was used to correct for the optical scattering of light in bands 1 through 4. A subset of the calibrated reflectance data was then extracted to cover the NPRA study area.

Spectral analysis of training areas was used to define spectral map units, which are referred to in this report as "spectral units." Landsat 7 ETM+ data were used to identify specific materials, or mixtures of materials, on the basis of their spectral characteristics and field data obtained from the study area in July 2004. Laboratory spectra (resampled to Landsat 7 ETM+ bandpasses) of typical materials found at NPRA (such as green vegetation, quartz sand, dead vegetation, and montmorillonite clay) have distinct spectral signatures that can be mapped using spectral shape-fitting algorithms (fig. 2). Image spectra used to define spectral units contain mixtures of green vegetation, quartz sand, dead vegetation, and clay and

[1]U.S. Geological Survey, Reston, VA 20192
[2]U.S. Geological Survey, Flagstaff, AZ 86001
[3]Bureau of Land Management, Fairbanks, AK 99709

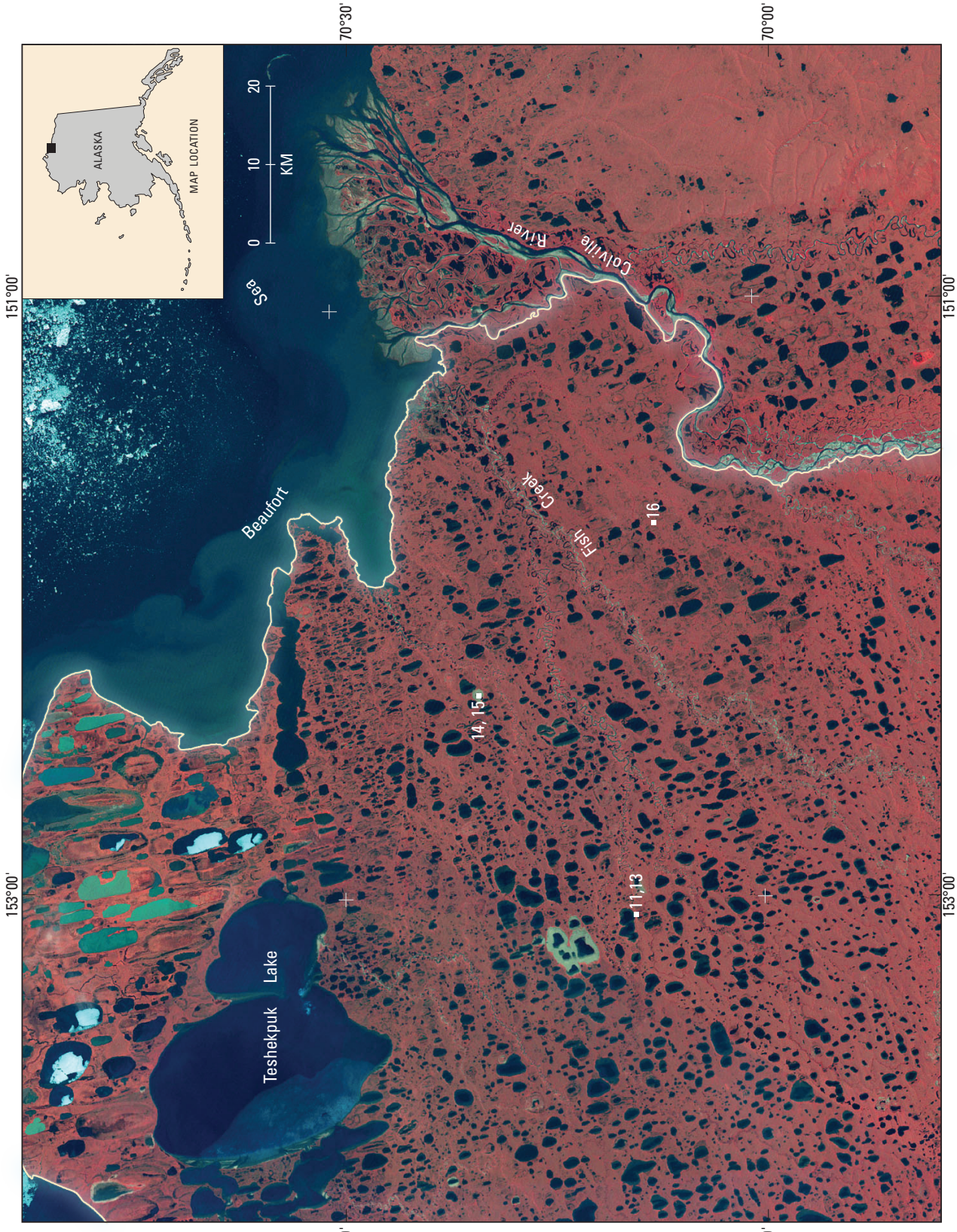


**Figure 1.** Landsat Multispectral Scanner false-color composite image (red=6, green=5, blue=4) of the Fish Creek study area, National Petroleum Reserve, Alaska (NPRA). Numbered points represent locations of photographs in this report (figs. 11, 13, 14, 15, 16). NPRA border is shown in white. Ice in some of the freeze-thaw lakes appears white in the image. Shallow or turbid water in some of the freeze-thaw lakes appears light green in the image. Meter grid based on Alaska Albers Equal Area coordinate system.

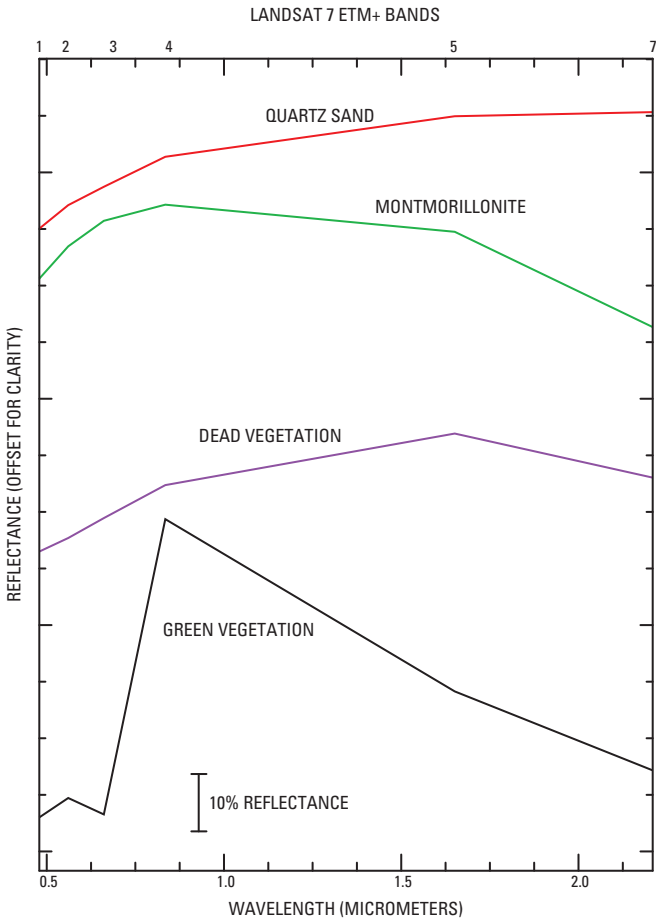


**Figure 2.** Graph showing U.S. Geological Survey laboratory spectra (Clark and others, 2003) of live (green) vegetation, dead (brown) vegetation, quartz sand, and montmorillonite, resampled to Landsat 7 ETM+ bandpasses.

thus have spectral signatures that consist of multiple spectral features.

Freeze-thaw lakes still contained a substantial amount of ice as well as water when the image was acquired in June 2003. ETM+ reflectance image spectra of sediment, vegetation, water, and ice show that bands 1 through 4 have low reflectance whereas band 5 (1.65 μm) reflectance for ice and water are lower, than the band 5 reflectance for vegetation and sediment (fig. 3). Thus, on the basis of water, ice, and vegetated sediment spectra, a threshold of ETM+ band 5 was used to map the freeze-thaw lakes and other water and ice bodies (fig. 4).

An image spectrum from the study area and a resampled spectrum of green vegetation from a spectral library both indicate a chlorophyll absorption feature at 0.66 μm (figs. 2 and 5). A Landsat 7 ETM+ band ratio of 4:3 produces an image with high digital number (DN) values where there are relatively strong chlorophyll absorption features; thus, the green vegetation spectral unit was mapped by applying a threshold to an ETM+ band ratio 4:3 image. Areas classified as the green vegetation spectral unit contained more than 50 percent green vegetation on the basis of field observations.

In order to map additional surficial units, a false-color-composite (red=band 7, green=band 4, blue=band 2) ETM+ image was assessed to select image spectra (fig 6*A*). Due to high spectral contrast, an ice and water mask was applied to the false-color-composite image to improve spectral variability. Spectral units other than green vegetation and water were defined by examining the spectral characteristics of image spectra (fig. 6*B*) associated with specific geomorphic features such as dunes, river bars, and lake shorelines (fig. 6*A*). Selection of specific landforms was based on inferred sediment types associated with the depositional environment that produced the landform, and from the 1:250,000-scale engineering geologic map of the study area (Carter and Galloway, 1985, 2005; Boggs, 1995; fig. 6*A*). Approximately 20 image spectra were selected from the false-color-composite ice- and water-masked image. Interpreted spectral units using this process include (1) vegetated, dry sand from linear ridges; (2) clean sand from active dunes around freeze-thaw lakes; (3) muddy sand from sand bars in rivers; and (4) wet, vegetated, sandy mud from lake sediments in freeze-thaw lakes (fig. 6*A*, *B*).

Matched filtering, an algorithm for detecting target spectra in the presence of spectral mixtures (Harsanyi and Chang,

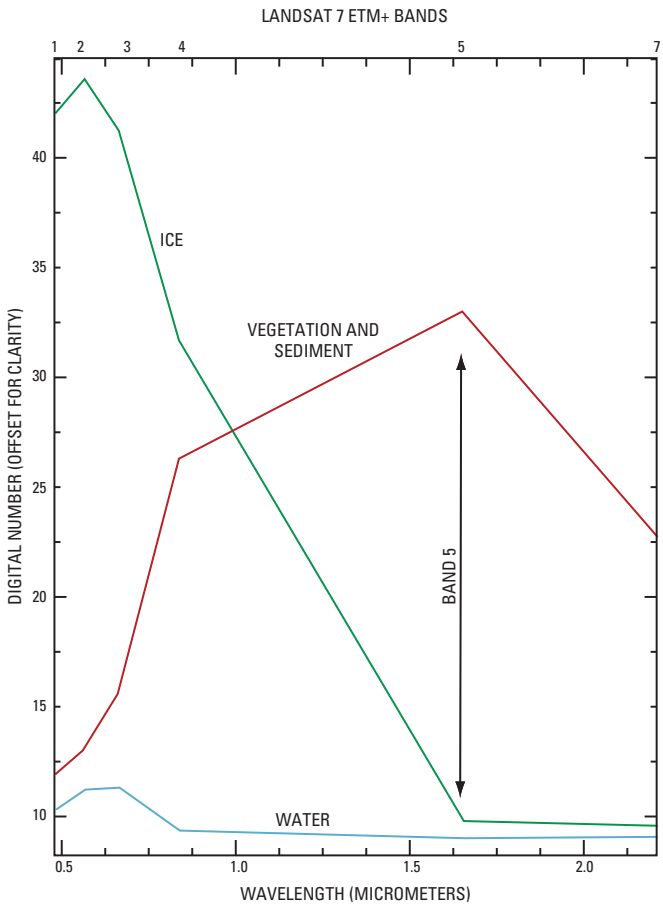


**Figure 3.** Graph showing Landsat 7 ETM+ image-reflectance spectra from the NPRA study area of water (blue line), ice (green line), and vegetation and sediment (red line). Band 5 illustrates more spectral contrast between water and ice and vegetation and sediment than all other Landsat 7 ETM+ bands.

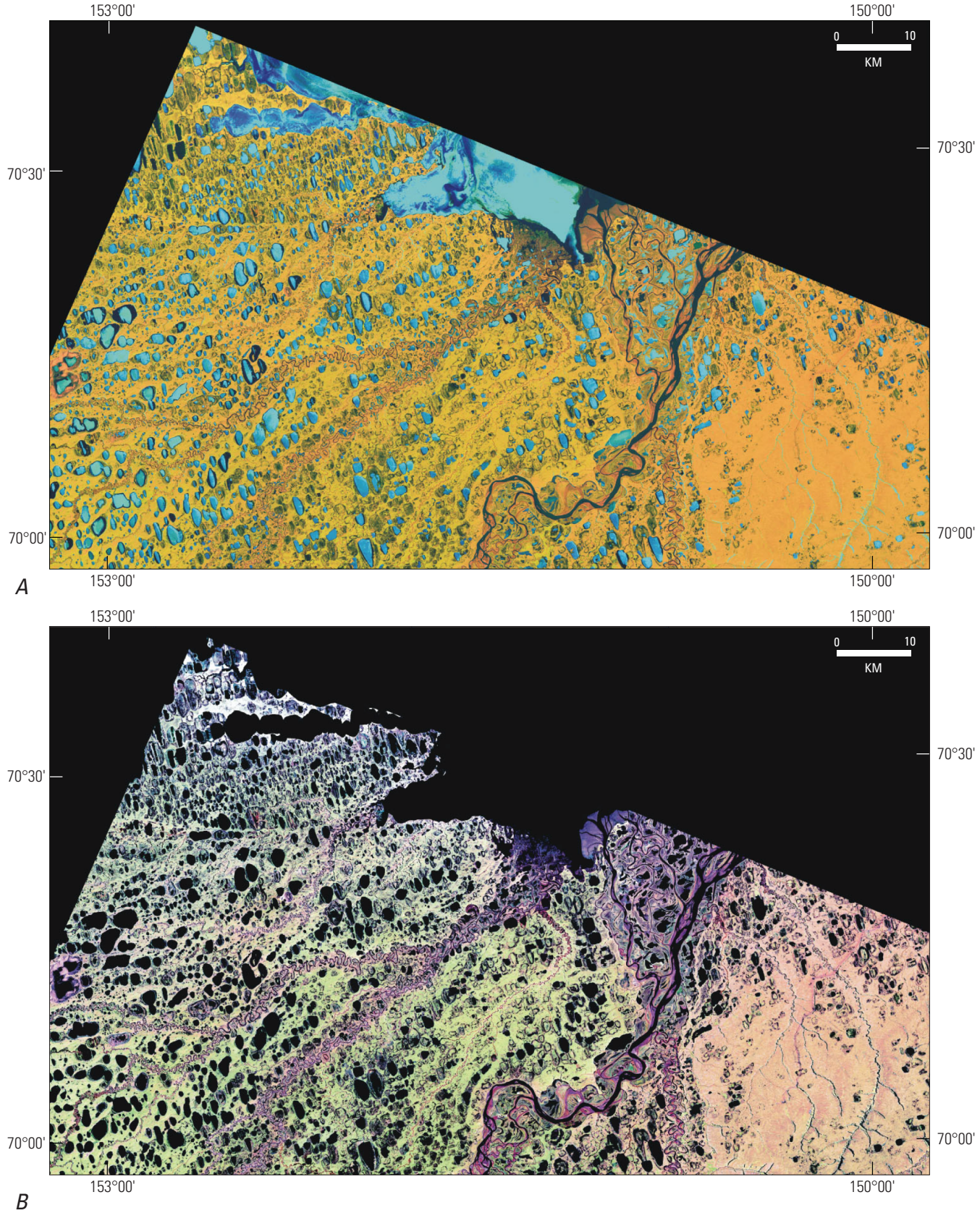


**Figure 4.** Landsat 7 ETM+ (red=7, green=4, blue=2) false-color composite images of the eastern part of NPRA. *A*. Unmasked image. *B*. With water and ice masked out using a band 5 threshold. Ice and water have high and low reflectance, respectively, which tends to obscure land features that have moderate reflectance. Thus, it is easier to see land features in the water and ice masked image *B* than the unmasked image *A*.

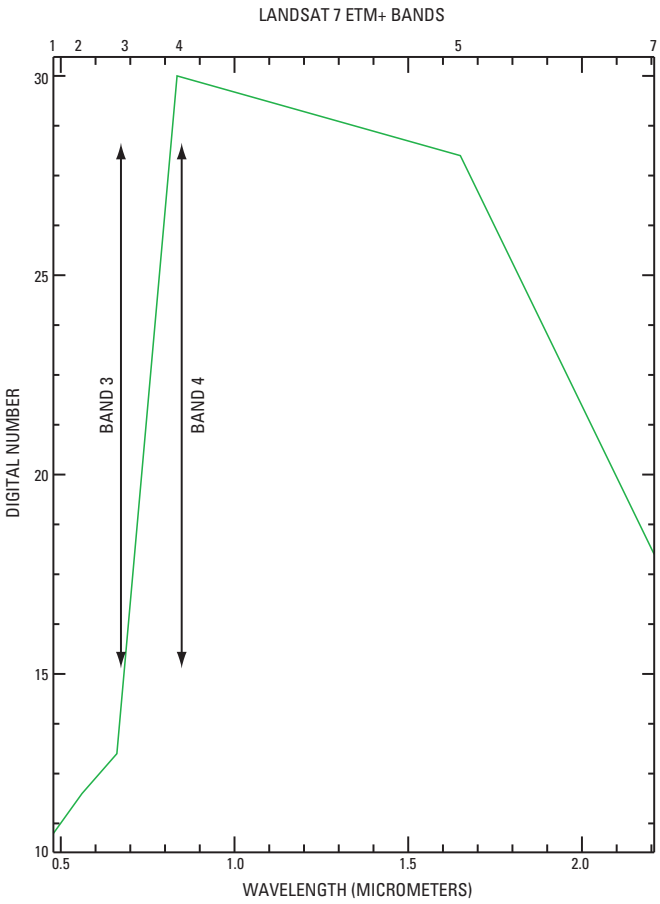


**Figure 5.** Landsat 7 ETM+ image-reflectance spectrum of green vegetation from NPRA illustrating low reflectance for band 3 (0.66 µm) and high reflectance for band 4 (0.82 µm). The 0.66 µm absorption feature is caused by chlorophyll.

1994; Farrand and Harsanyi, 1997), was used with the image spectra to produce a series of gray-scale images (figs. 6B and 7). The images were qualitatively assessed for spatial coherence and accuracy (fig. 7). Four images were selected and interpreted to represent mixtures of sediment, water, and vegetation on the basis of (1) their spectral properties, (2) similar distribution in relation to lithologic units of the geologic map (Carter and Galloway, 1985, 2005), (3) a 5-m-resolution digital-terrain model of the IFSAR data, and (4) the water-masked false-color-composite RGB Landsat 7 ETM+ image (figs. 2, 3, 5, and 6; sheet 1). A threshold was applied to each gray-scale image to remove noise, poor matches, and similarly mapped pixels. The remaining pixels in the gray-scale images were converted to vectors. The vector spectral units for each processed image were then combined on a Landsat band 5 image to produce a provisional surface-classification map.

The provisional surface-classification map was tested in the field for consistency and accuracy of the spectral units with respect to surficial material assignments such as sediment, water, and vegetation content. A FieldSpec Pro[4] field spectrometer was used to collect reflectance spectra in the field and was used to collect reflectance spectra from field samples in the laboratory. The field spectrometer collects reflectance data at 1-nanometer spacing from 0.35 µm to 2.5 µm. A comparison of field spectra with lab spectra from selected calibration sites consisting primarily of windblown quartz sands indicated that no additional calibration of the ETM+ dataset was necessary. The field and lab spectra also were compared to the image spectra for evaluation of material content and accuracy of spectral units.

## IFSAR Data

The IFSAR data used in the study were collected by the STAR-3i[5] airborne synthetic aperture radar system. STAR-3i is a high-resolution, single-pass, across-track IFSAR system, which uses two apertures to collect data from the surface. The path-length difference between the apertures for each image point, along with the known aperture distance, is used to determine the topographic height of the terrain. The IFSAR system is capable of collecting data with a vertical accuracy of less than 1 m and a horizontal accuracy of less than 3 m.

Data are delivered as three core products: orthorectified radar images (ORRIs), digital surface models (DSMs), and digital terrain models (DTMs). ORRIs are 8-bit grayscale GeoTIFF images that show the radar reflectance intensity of various earth surface materials. These images are commonly used to identify and extract drainage networks and cultural features such as pipelines, roads, and buildings. The ORRIs used in this study had a pixel size of 1.25 m and a horizontal accuracy of 2.5 m. The DSMs, or "first-return" elevation data, display the first surface on the ground that the radar strikes. These images consist of measured points collected by the sensor, including the z-values of structures (for example, heights of building and towers) and vegetation (for example, trees and crops). These elements are removed from the DSM through filtering techniques to create a DTM. The DTMs, or "bald-earth" elevation data, are similar to digital elevation models (DEMs) in that nonterrain elements are absent (fig. 8). Unlike the regular array of elevation values that are characteristic of a DEM, however, a DTM defines topographic elements by irregularly spaced breaklines, or abrupt changes in surface smoothness, such as shorelines, roads, streams, and slope breaks. The result is a more accurate depiction of the terrain, which is useful for contouring, triangulated irregular network (TIN) calculations, and other terrain modeling (fig. 9).

## Color Shaded-Relief, and Shaded-Relief Surface-Classification Maps

Computer-based analytical hillshading has become a widely used tool to visualize three-dimensional topography

[4]Fieldspec Pro—Analytical Spectral Devices, Inc., 5335 Sterling Drive, Suite A, Boulder, CO 80301 USA

[5]Star-3i—Intermap Technologies, Inc., 8310 South Valley Highway, Suite 400 Englewood, CO 80112-5847 USA

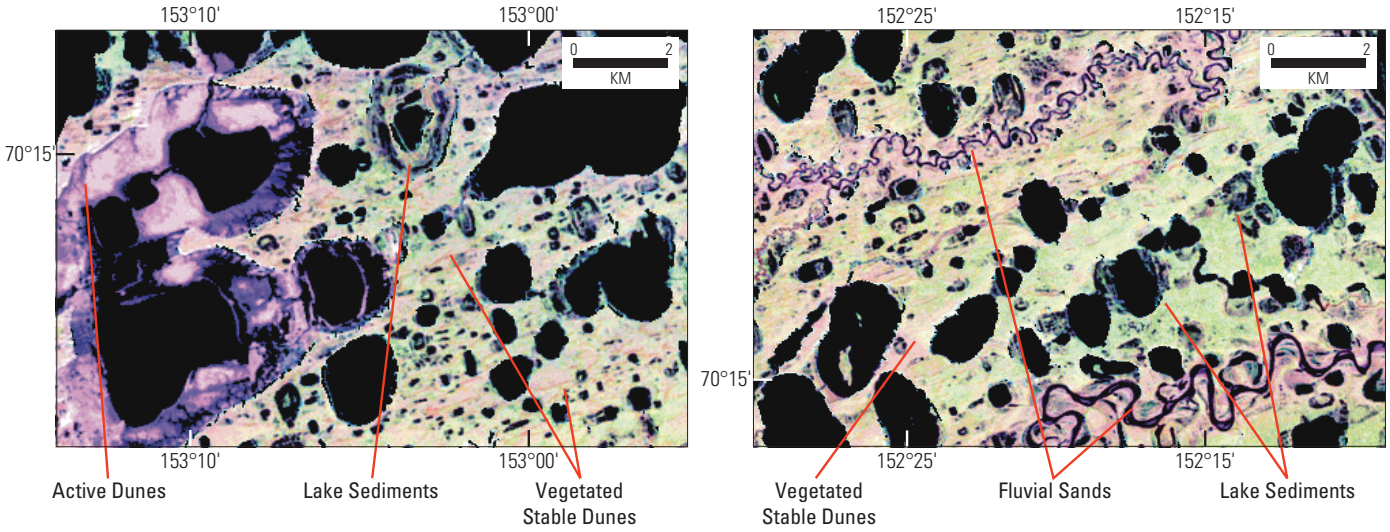


*A*

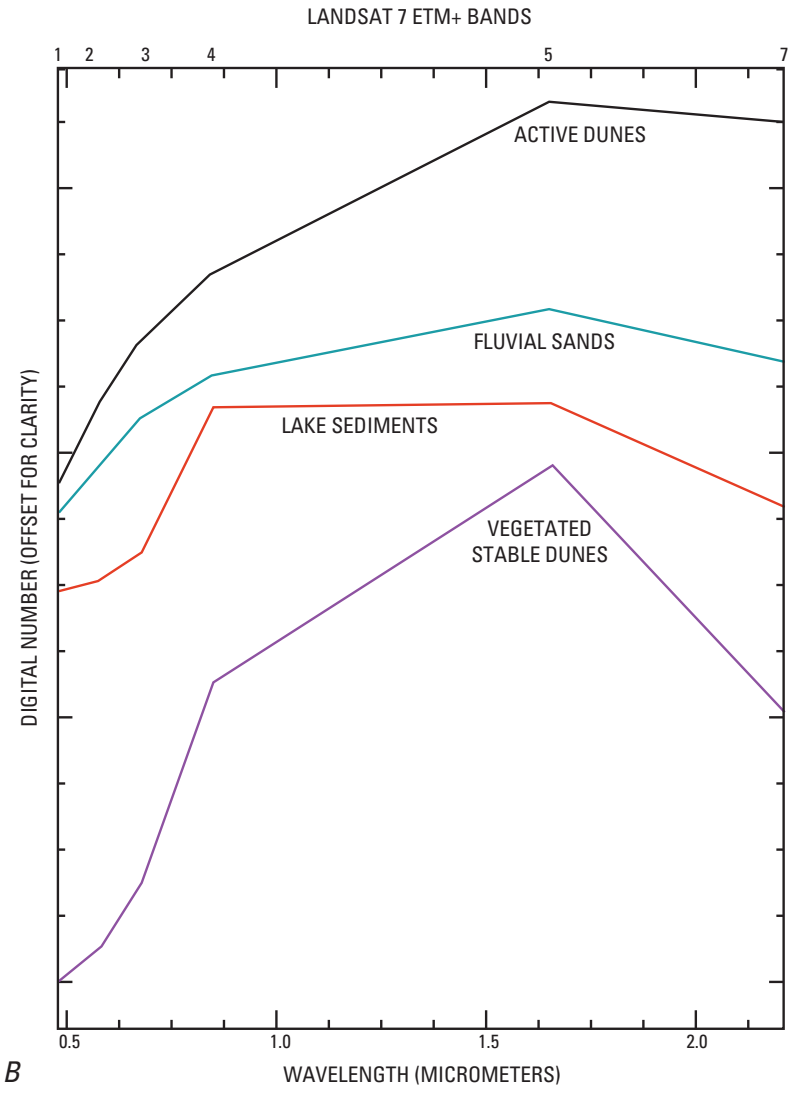


*B*

**Figure 6.** Images used to identify landforms and associated spectra. *A*, Water- and ice-masked Landsat 7 ETM+ false-color composite (red=7, green=4, blue=2) images used to identify landforms such as lakes, active and vegetated dunes, and fluvial systems. *B*, Image spectra selected from the identified landforms in part *A*.

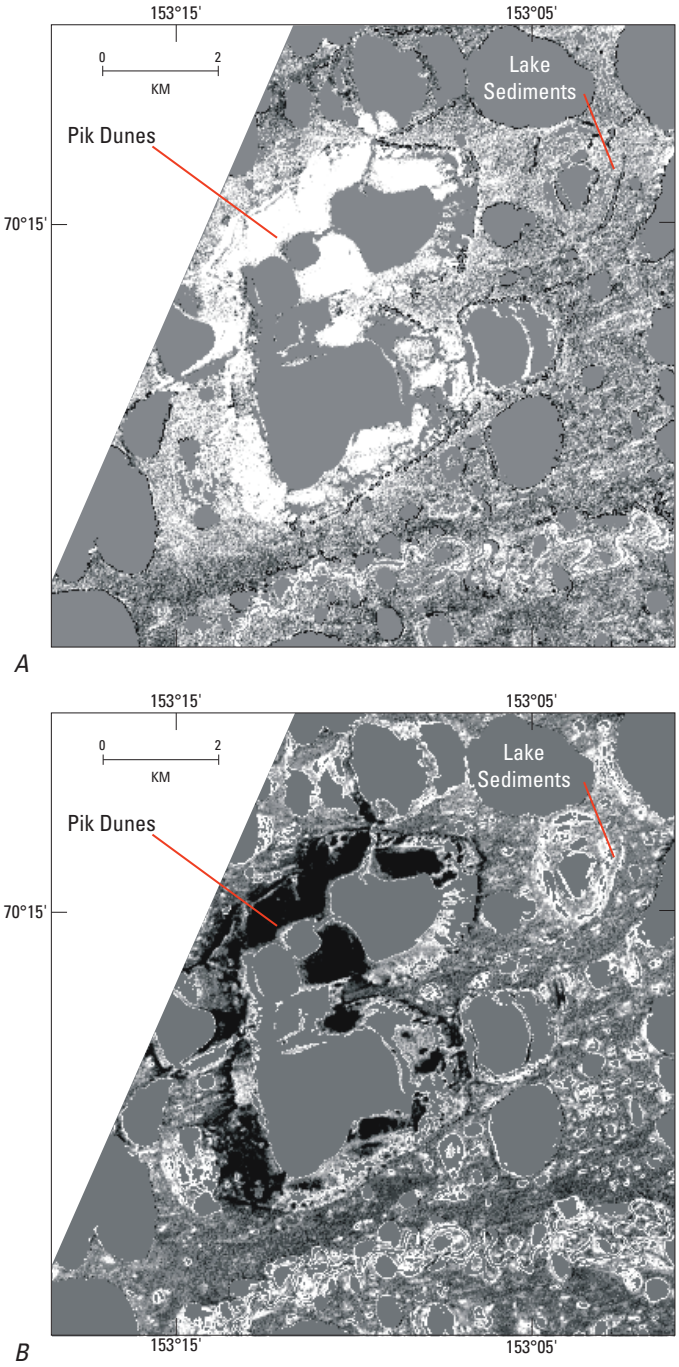


**Figure 7.** An example of matched filtering results on two lake-sediment image spectra from NPRA (in the far left of the imagery shown on plates 1-3). White pixels represent a good match of the input spectrum to image spectra and black pixels represent a poor match. *A*, Matched filter image has poor spatial coherence in mapping lake sediments and has incorrectly mapped the Pik Dunes. *B*, Matched filter image has correctly mapped the lakes sediments and has good spatial coherence.

on a two-dimensional surface. Unlike manually produced shaded-relief maps, analytical hillshade images often reveal imperfections in the elevation data used to render the image. The IFSAR data contained flaws in some areas because excess motion in the aircraft caused visible ripples in the image. A regular banding pattern was apparent along the sensor swath boundaries when the elevation data were viewed at small scales. Even with these flaws, the DSMs and DTMs derived from the IFSAR system proved to be an excellent data source for generating the shaded-relief and surface-classification images (Garrity, 2004).

Large-scale (1:20,000) shaded-relief images were generated from DTM data in order to identify the location of surficial objects with greater accuracy. The initial image rendering revealed potential challenges related to the portrayal of surface features in an area devoid of any significant relief. When rendered with no vertical exaggeration, the shaded-relief image was essentially flat. Using a 5× vertical exaggeration, the shadows appeared blocky at the desired map scale. To give the landscape images a more natural appearance, DTM surfaces were slightly "bump-mapped" (Garrity, 2004). Because the images were used for surface delineation, a random height map was unsuitable for fear of compromising data integrity. Instead, the corresponding DSM was used as a height map to generate the bumped surface. The natural "roughness" of the DSM gave the hillshaded DTM a subtle texture without obscuring the DTM surface with unnecessary detail.

Removal of the jagged shading was accomplished by generalizing the raw data grids, isolating their shaded pixels, and then merging the generalized shaded layer with the original grid. In order to generalize the raw data grids, softening techniques were applied in ArcInfo Workstation[6] using focal functions. The amount of softening was regulated by adjusting the neighborhood configuration (shape, size) in the focal command. In all instances, a very small neighborhood was used and care was taken not to overgeneralize the softened grids. The isolation of shaded pixels within the generalized grids was accomplished in Adobe Photoshop[7] by using the "Curves" tool; the remaining pixels were converted to white. Finally, the adjusted softened hillshade and the original hillshade were merged by multiplying the two images in Photoshop. Multiplying the images caused the converted white pixels of the softened image to drop out, which in turn resulted in a softening effect that was restricted to the darkest shades of the merged image. The final resulting hillshade image has a more natural appearance, devoid of any jagged shading.

The 30-m-resolution surface-classification map was resized to match the dimensions of the 5-m-resolution DTM hillshade image in ERDAS Imagine[8]. A median filter was applied to the 30-m-resolution dataset to minimize pixelization when the image is viewed at full resolution. Datasets were fused (merged) using raster arithmetic operators in ArcGrid[6] and then downsampled appropriately based on the desired map scale.

[6]ArcInfo Workstation and ArcGrid—Environmental Systems Research Institute, Inc., (ESRI), 380 New York Street, Redlands, CA 92373 USA
[7]Photoshop—Adobe Systems Inc., 345 Park Avenue, San Jose, CA 95110-2704 USA
[8]ERDAS Imagine—Earth Resources Data Analysis System, Leica Geosystems Geospatial Imaging, LLC, 5051 Peachtree Corners Circle, Norcross, GA 30092-2500 USA

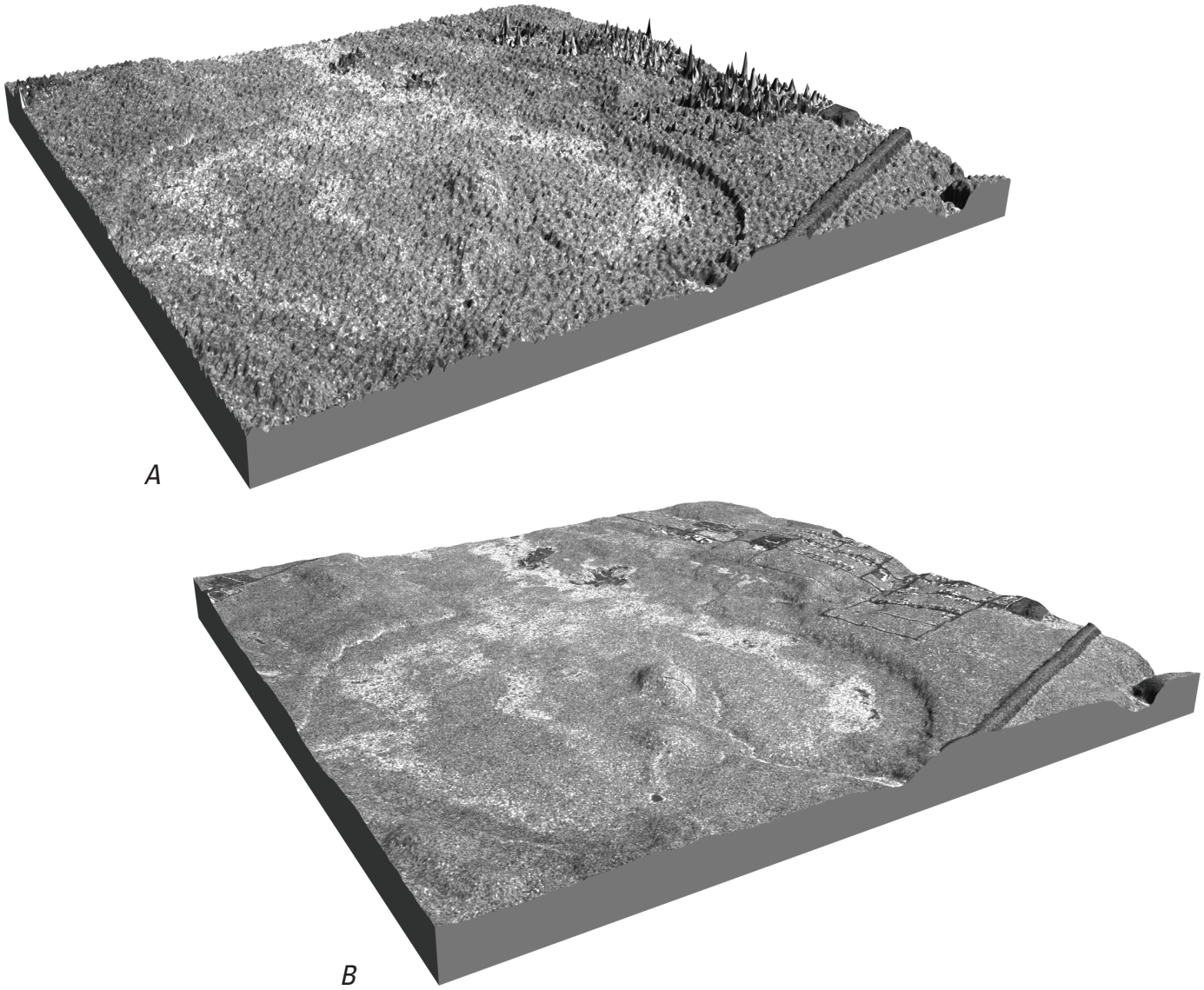


**Figure 8.** Block diagrams of the Nuiqsut area in eastern NPRA. *A*, Digital surface model (DSM) draped with an orthorectified radar image (ORRI). *B*, Digital terrain model (DTM) draped with an ORRI. The DSM displays all of the measured points collected by the sensor, as illustrated by the irregular elevation spikes in the diagram. The nonterrain elements are removed through filtering in order to create a DTM. The DTM simulates a "bald-earth" and is traditionally preferred over a DSM for topographic mapping purposes (Garrity, 2004).

# Interpretation

## Surface-Classification Map

The spectral units of the ETM+ surface-classification map are as follows: water (blue); green vegetation (green): dry, vegetated sand (yellow); wet, vegetated, sandy mud (red); clean sand (white); and muddy sand (cyan) (sheet 2). In addition, unclassified pixels (black) are shown on the classification map.

The average spectrum of the wet, vegetated, sandy mud spectral unit (red on the surface-classification map) has a strong band 3 absorption feature, a high reflectance in band 5, a low reflectance in band 7, and a relatively low albedo when compared to other spectral units (fig. 10). Field observations indicate that the wet, vegetated, sandy mud spectral unit consists of approximately 45 to 50 percent water, approximately 45 to 50 percent dead or senescent (brown, no chlorophyll present) and live (green, chlorophyll present) grass, and less than 5 percent sandy mud at the surface (fig. 11). Field spectra resampled to ETM+ bandpasses are very similar to the image spectra that were taken from parts of the image classified as wet, vegetated, sandy mud. The field spectra illustrate a strong (0.7 μm) chlorophyll absorption feature, and low reflectance in the 2.0 μm to 2.5 μm region due to cellulose absorption from dead and live vegetation, and from water (fig. 11; red curve on fig. 12). The field spectra also have a lower albedo than other field spectra due to the presence of water (figs. 3 and 11).

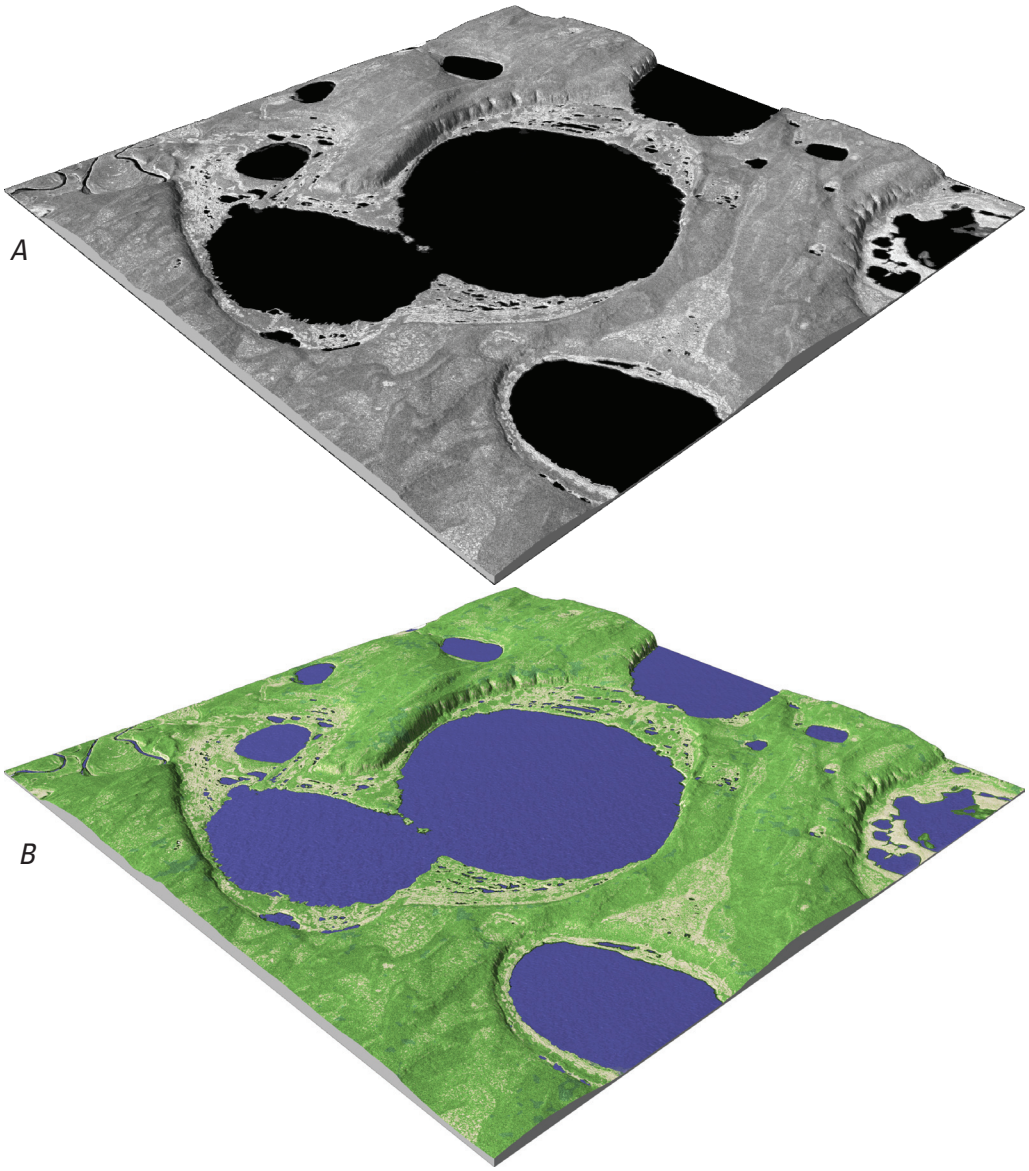


**Figure 9.** Block diagrams of freeze-thaw lakes in eastern NPRA. Both are digital terrain models (DTMs) draped with orthorectified radar images (ORRIs). *A*, DTM draped with a grayscale ORRI. *B*, DTM draped with colorized ORRI. The colors were derived from Landsat 7 ETM+ image data which were processed to identify surface materials.

Thus, the spectral characteristics of the wet, vegetated, sandy mud spectral unit are due to a mixture of live (green) and dead or senescent (brown) vegetation (low reflectance in bands 3 and 7, respectively), and water (relatively low albedo compared to other spectral units).

The average spectrum of the dry, vegetated sand spectral unit has a slight chlorophyll absorption feature, high band 5 reflectance, low band 7 reflectance, and the highest albedo of all of the spectral units (fig. 10). Field data indicate that the dry, vegetated sand unit consists of approximately 20 percent live (green) vegetation, 75 percent dead (brown) vegetation, and less than 5 percent bare sand (fig. 13). In some areas (such as on parabolic dunes), the dry, vegetated sand spectral unit consists of up to 20 percent lichen and up to 20 percent bare sand (fig. 13). A field spectrum illustrates a 0.7-μm (ETM+ band 3) chlorophyll absorption feature. The field spectrum also illustrates high reflectance in the 1.4- to 1.8-μm region and low reflectance in the 2.0- to 2.5-μm region, which is due to cellulose absorption (figs. 12*A* and 10, purple curve). Quartzose sand also has high reflectance in the 1.4 to 1.8 μm region (figs. 2 and 10), which is partially responsible for the high band 5 reflectance of image spectra from the dry, vegetated sand spectral unit. The spectral characteristics of the dry, vegetated sand spectral unit are due to small amounts of live (green) vegetation mixed with large amounts of dead or senescent (brown) vegetation, sand, and lichen.

Spectral comparisons of an averaged field spectrum (n=15) resampled to Landsat 7 ETM+ bandpasses and the average image spectrum of the dry, vegetated sand spectral unit indicate that band 5 and band 3 reflectances are lower for field spectra; however, the overall spectral shapes are similar (fig. 12*B*). The field spectrum of dry, vegetated sand is similar to the field spectra taken from an area that is classifed as wet, vegetated sandy mud (fig. 12). The lower band 3 and band 5 reflectance values of the field spectrum resampled to Landsat 7 ETM+ bandpasses are due to the seasonal changes in vegetation. The field spectra were recorded in midsummer when there was more live (green) vegetation than in early

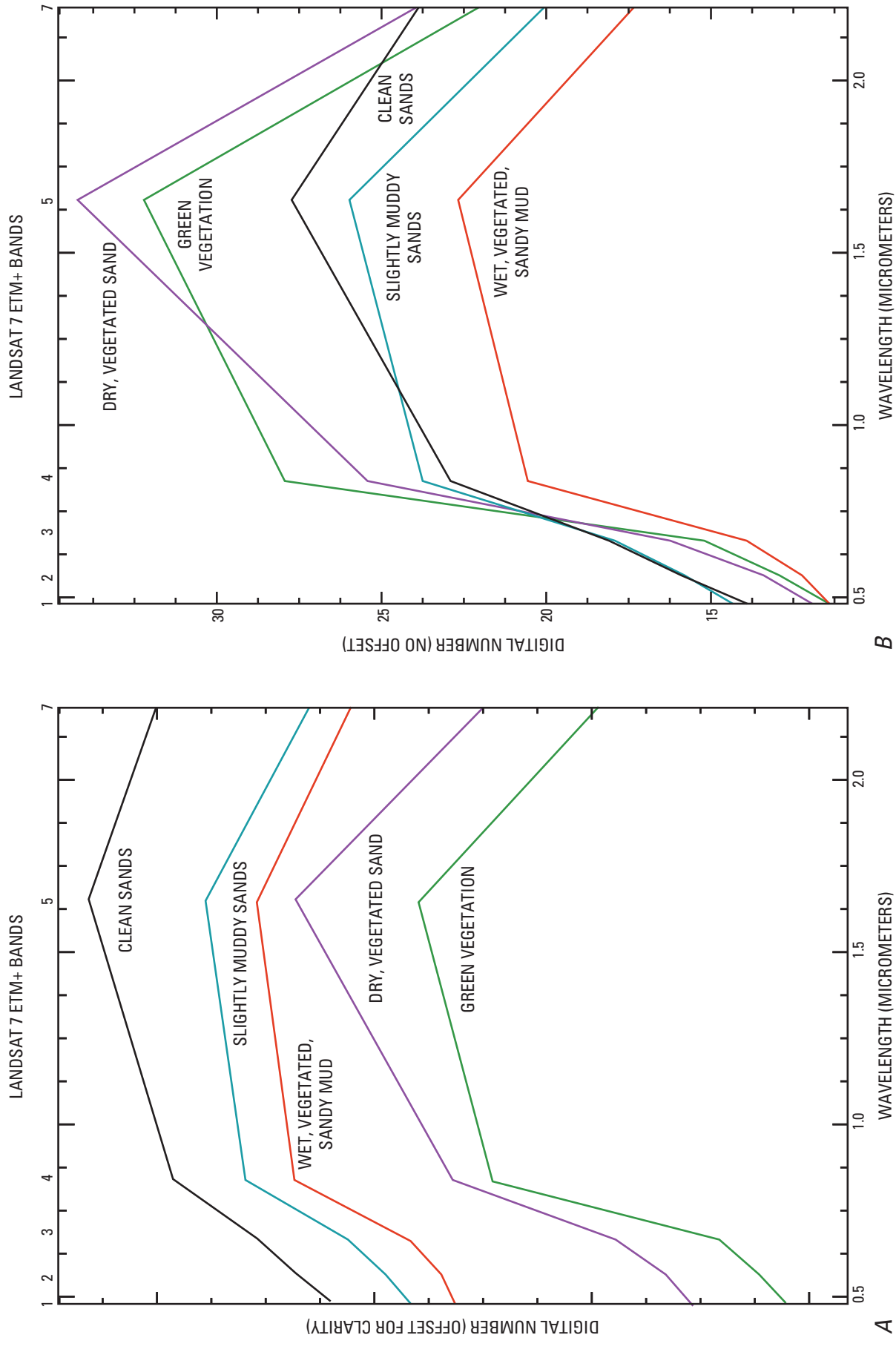


**Figure 10.** Offset and nonoffset averaged image spectra of spectral units from NPRA Landsat 7 ETM+ dataset . *A*, Averaged image spectra offset for comparison of spectral features. *B*, The same averaged image spectra not offset in order to compare albedo.

**Figure 11.** Photograph of water, sandy mud, and dead and green grass taken in the western part of the NPRA study area. The area shown in the photograph is mapped as wet, vegetated, sandy mud and is shown by red pixels on sheets 2 and 3. See figure 1 for location of this photograph. Lens cap in lower left of photograph is for scale. Photograph by John C. Mars.

summer when the Landsat 7 ETM+ data were acquired. Green vegetation contains more chlorophyll and water than dead or senescent (brown) vegetation, and results in lower reflectance in bands 3 and 5 (figs. 2, 12, and 13). The increase in green vegetation later in the summer indicates that the acquisition of data by visible to short-wave infrared detectors needs to occur in early summer when vegetation is still senescent.

The average image spectrum for the clean sand spectral unit has a small chlorophyll absorption feature, high reflectance in bands 5 and 7, and lower albedo when compared to the average dry, vegetated sand spectrum (fig. 10). The lower albedo of the clean sand average image spectrum may be due to surface moisture at the time of the Landsat data acquisition. Field observations indicate that the clean sand spectral unit primarily consists of quartz sand (approximately 95 percent) and minor amounts (less than 5 percent) of live (green) vegetation, silt, and clay (fig. 14). Quartz is spectrally flat and has high reflectance in the 1.5- to 2.4-μm region (fig. 2). Laboratory spectra of sand samples from dune blowout features indicate high reflectance, from 1.5 to 2.5 μm, with slight 2.20 μm and 2.35 μm absorption features due to muscovite (fig. 12). The high reflectance of bands 5 and 7 in the average spectrum of the clean sand spectral unit is due to the high percentage of quartz (greater than 95 percent; figs. 2 and 12).

The slightly muddy sand spectral unit has a more intense absorption of band 7 than the clean sand spectral unit, and a less intense chlorophyll absorption and higher albedo than the wet, vegetated, sandy mud spectral unit (fig. 10). Laboratory spectra of all of the sands from the study area have a 2.2-μm absorption feature that is typically associated with either muscovite, illite, or montmorillonite (figs. 2 and 10). Field observations also indicate that there is slightly more (greater than 5 percent) silty mud and green vegetation in the muddy sand spectral unit than in the clean sand spectral unit (fig. 15) but less than in the wet, vegetated, sandy mud spectral unit. The greater percentage of clay and (or) muscovite and green vegetation accounts for the deeper band 7 absorption feature in the slightly muddy sand unit than observed in the clean sand spectral unit.

Some pixels did not correlate with any of the spectral unit classifications. Field investigations in June 2004 indicated that some of the nonclassified areas contained equal amounts of green and dead or senescent vegetation and up to 10 percent standing water (fig. 16). It was not possible to determine if this is a separate classification unit. Many of the nonclassified pixels have different spectral signatures; therefore, several different spectral classes may be grouped in the nonclassified category.

A single spectral unit, a combination of spectral units, or a combination of spectral units and nonclassified pixels form patterns that define eolian, fluvial, deltaic, and marine depositional facies (sheet 2). The dry, vegetated sand spectra primarily correspond to deposits of eolian and marine sand located in the northwestern part of the study area. The wet, vegetated, sandy mud spectral unit primarily defines the muddier lake sediments of freeze-thaw lakes. Clean sand and muddy sand spectral units correlate with recent sand bodies, including eolian blowout features, fluvial sand bars, and deltaic deposits. A mixture of (1) dry, vegetated sand, (2) green vegetation spectral units, and (3) unclassified pixels define flood-plain deposits in the eastern part of the study area.

On the basis of both field and spectral data, most of the spectral characteristics observed in the NPRA imagery are due to water, quartz sand, silty mud, live (green) vegetation, and dead or senescent (brown) vegetation. The primary spectral controls on the dry, vegetated sand are mixtures of live (green) and dead or senescent (brown) vegetation. The freeze-thaw lake sediment's spectral characteristics are primarily due to mixtures of live (green) vegetation, dead or senescent (brown) vegetation and water. The clean sand spectral unit's characteristics are due primarily to quartz sand, and the muddy sand

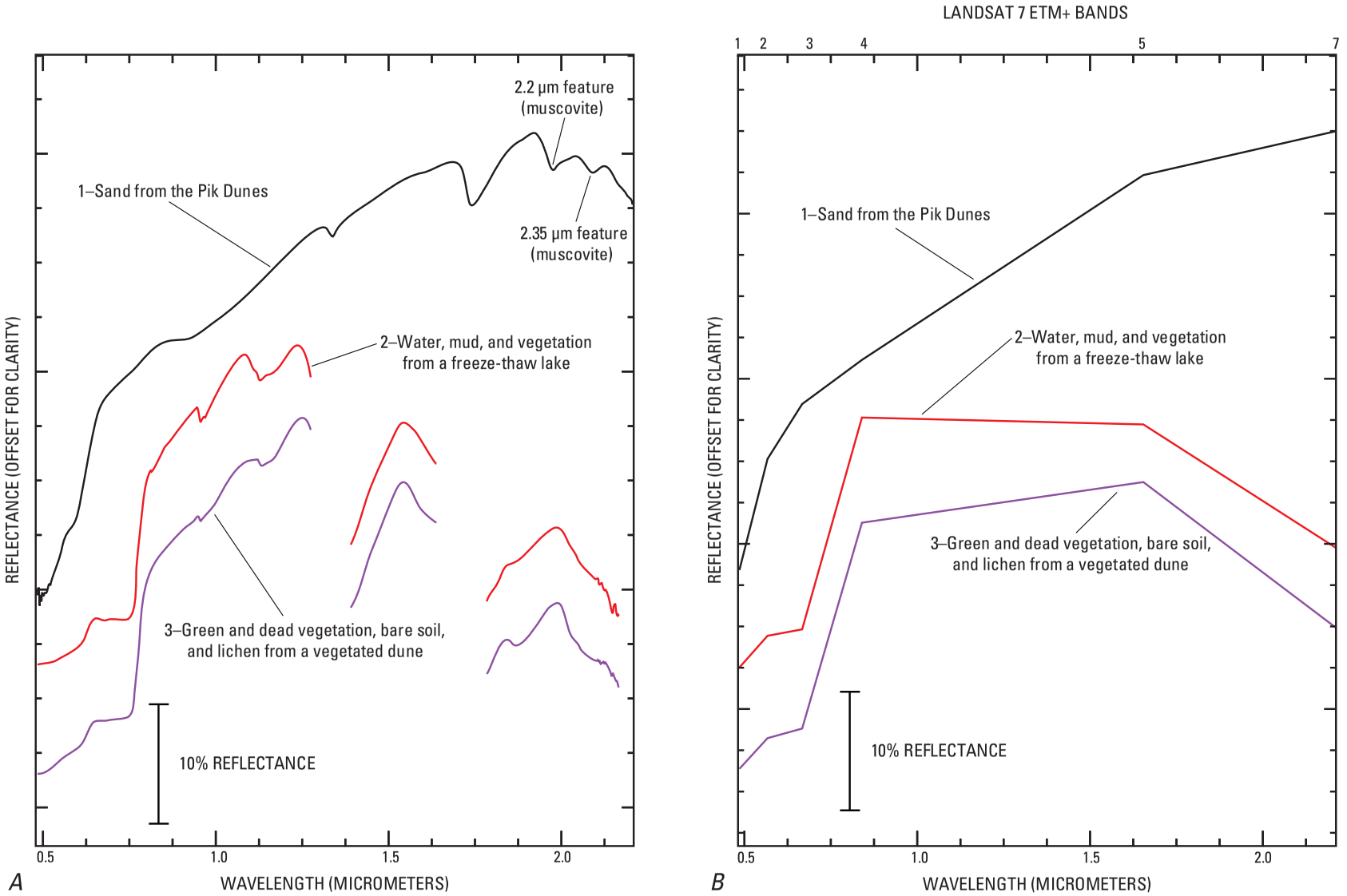


**Figure 12.** Laboratory and field spectra from NPRA. *A*, (1) Laboratory spectrum of sand from the Pik Dunes; the 2.2 µm absorption feature is caused by less than 5 percent muscovite content of the sand. (2) An averaged spectrum produced from 20 field spectra of lake vegetation, sediment, and water; the red line represents the wet, vegetated, sandy mud spectral unit; vegetation spectral characteristics include the 0.66 µm absorption feature, which is caused by chlorophyll and the 2.165 µm and 2.3 µm absorption features, which are caused by cellulose. (3) An averaged spectrum using 10 field spectra collected from an eolian dune that was covered by green and dead vegetation, bare soil, and lichen; the purple line represents the dry, vegetated sand spectral unit; chlorophyll and cellulose absorption features due to vegetation are present in the spectra. *B*, (1) Spectrum 1 from part *A* resampled to Landsat 7 ETM+ bandpasses. (2) Spectrum 2 from part *A* resampled to Landsat 7 ETM+ bandpasses. (3) Spectrum 3 from part *A* resampled to Landsat 7 ETM+ bandpasses.

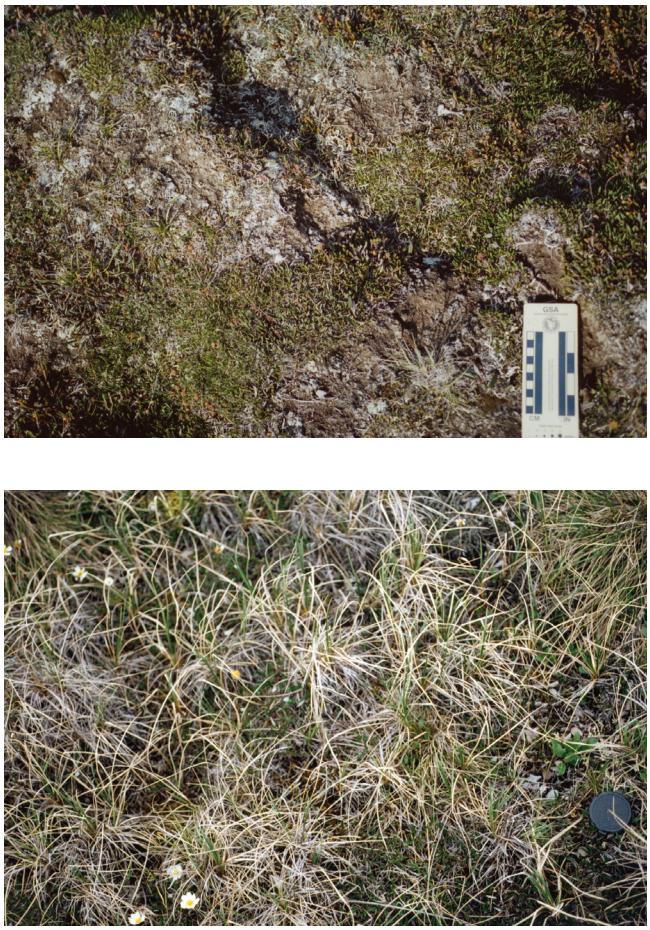

**Figure 13.** Photographs of vegetation on dunes in NPRA. *A*, Photograph of moss lichen and bare soil on the crest of a parabolic dune situated on top of a larger eolian dune in the western part of the NPRA study area. Scale at the lower right of photo contains vertical dashed lines with centimeters on the left and inches on the right. *B*, Photograph of green and dead sedge on an eolian dune. The areas in which parts *A* and *B* were photographed are classified as vegetated sand spectral units which is the yellow unit on the surface classification and shaded-relief surface-classification maps, illustrated on sheets 2 and 3, respectively. Lens cap in lower left of the photograph is for scale. The location of the photograph is shown in figure 1. Photograph by John C. Mars.

spectral unit's characteristics are due primarily to quartz with small mixtures of silty mud and vegetation.

## Shaded-Relief Surface-Classification Map

The shaded-relief surface-classification map was produced by integrating the 5-m resolution IFSAR data with the ETM+ surface-classification map (sheet 3). The colors for the classification scheme are the same as for the surface-classification map; however, light-gray to black hillshading from the DTM has been added to enhance surface features.

Specific spectral units, or combinations of spectral units, tend to correlate with specific topographic features such as eolian and coastal ridges and river valleys. A combination of shaded-relief data with the pixels representing dry, vegetated sand, sandy mud, and nonclassified pixels define the east- to northeast-trending ridges that are capped by parabolic dunes in the western part of the study area (sheet 3). Pixels classified as dry, vegetated sand primarily cover the ridges and dunes; pixels that are nonclassified and pixels classified as wet, sandy mud dominate the inter-dune and inter-ridge areas (sheet 3).

River valleys with profiles of less than 10 m dominate the eastern part of the study area (sheet 3). Meandering channels are slightly incised and the sediments in the active channels are classified primarily as clean or slightly muddy sands. Adjacent to the active fluvial channels are low-profile water- and sediment-filled abandoned channels and freeze-thaw lakes; these areas are classified as water, or as wet, vegetated, sandy mud (sheet 3). Bordering the active and abandoned channels are low-relief terraces that are classified as dry, vegetated sand (sheet 3). Field investigations indicate that reworked windblown fluvial deposits cap some of the low-relief terraces. Flanking the low-relief terraces are broad, flat, interfluvial plains that are classified as either wet, sandy mud, dry, vegetated sand; or green vegetation; these areas also include nonclassified pixels (sheet 3). The broad plains contain an abundance of sandy mud and water-filled freeze-thaw lakes. Some of the lakes and lake deposits tend to form groups of northeast-trending, topographically low areas and may indicate locations of older abandoned stream and river channels.

The shaded-relief surface-classification map illustrates a close relationship between surficial vegetation and topography, which may be linked to the availability of water for vegetation and the depth to permafrost. The DTM shows that the eolian and coastal ridges, which cover the western part of the study area, are up to 500 m wide, average 4 km in length, and have vertical profiles of approximately 18 m (sheets 1 and 3). Up to 60 percent of the vegetation on these dunes is either senescent or dead (brown to light-gray in color; fig. 14). Vegetation types on eolian and coastal ridges include sedges, lichens, and mosses (fig. 13). Field investigations show that the flood plains and river valleys in the eastern part of the study area contain up to 80 percent green vegetation, consisting of sedges, dwarf willows and alders, perennials, and mosses (fig. 16). Thus, field observations suggest that there is significantly more moist vegetation and standing water in the river valleys than on the eolian and coastal ridges. Shallow pits dug in the field indicate that the depth to permafrost is 0.5 to 1.2 m in the eolian and coastal dune areas, and 0.2 to 0.4 m in the eastern fluvial-dominated areas. The differences in depth to permafrost may be due either to better drainage of the eolian and coastal dune sediments, or to a greater exposed surface area of the dunes, which would increase the rate of melting permafrost. Because of the extremely dry conditions of less than 10 cm of precipitation per year (NOAA, 2005), water perched above the permafrost is a major source of water for vegetation. Thus, an increased depth to permafrost would create more arid surface conditions that favor stressed vegetation and organisms, such as lichens, that thrive in relatively arid conditions.

**Figure 14.** Photograph of a wind blowout feature in NPRA that consists of greater than 95 percent quartz sand. Note that there are some 1-m-high dunes with vegetation in the background. The area in the photograph is classified as the clean sand spectral unit, which is the white unit on the surface-classification and shaded-relief surface-classification maps, illustrated on sheets 2 and 3, respectively. The location of the photograph is shown in figure 1. Photograph by John C. Mars.

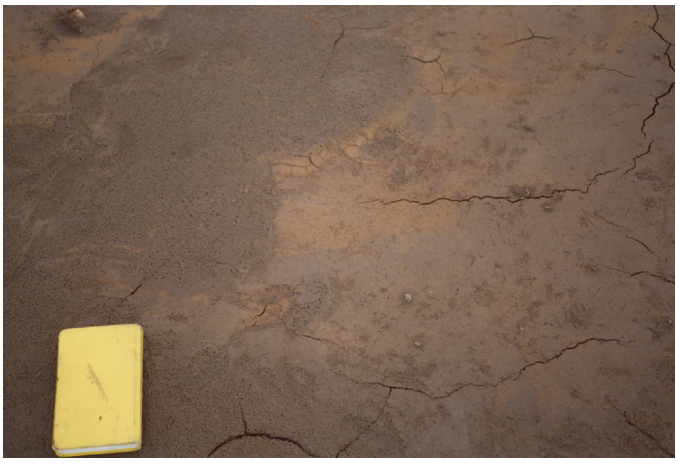

**Figure 15.** Photograph of a slightly muddy sand deposit (less than 95 percent quartz sand) at a drained freeze-thaw lake and blowout feature in the western part of the NPRA study area. The area in the photograph is classified as the slightly muddy sand spectral unit, which is the white unit on the surface-classification and shaded-relief surface-classification maps, illustrated on sheets 2 and 3, respectively. Notebook for scale. The location of the photograph is shown in figure 1. Photograph by John C. Mars.

## Conclusions

Image and field spectra indicate that the acquisition of visible and short-wave infrared remote-sensing imagery must be done during early summer. In mid- to late summer, green vegetation densities increase and obscure some of the spectral variability. In this study, the field spectra of dry, vegetated sand acquired in mid-summer resemble field spectra taken from lake deposits due to the increase in green vegetation. Image spectra of dry, vegetated sand acquired in early summer, however, indicates less green vegetation and has distinct spectral features that can be mapped.

**Figure 16.** Photograph of dead and green vegetation cover in a river valley in the eastern part of the NPRA study area. Most of the green vegetation is dwarf willow. Notebook for scale. This area is not classified as a specific spectral unit and is illustrated as the black unit on sheets 2 and 3. The location of the photograph is shown in figure 1. Photograph by John C. Mars.

The IFSAR and Landsat 7 ETM+ data provide complementary information that enhances the ability to map subtle land-cover variations in the NPRA coastal plain. The DTM permits identification of landforms using elevation data. The surface-classification map is composed of spectral units that define different types of sediment, such as wet, sandy mud, muddy sand, and clean sand. The spectral units of the surface-classification map also define areas of green vegetation, dead or senescent vegetation, and water during the early summer. The spectral units of the surface-classification map form distinct patterns that highlight geomorphic features such as sediment-filled lakes, dune and ridge complexes, and river valleys. The shaded-relief surface-classification map provides a better definition of topographic features than the individual datasets due to the relationship of topographic features, sediment types, and vegetation cover to water availability; water availability may be due to variations in the depth to permafrost for specific landforms.

## References Cited

Boggs, Sam, Jr., 1995, Principles of sedimentology and stratigraphy, second edition: Englewood Cliffs, N.J., Prentice Hall Inc., 774 p.

Carter, D.L., and Galloway, J.P., 1985, Engineering geologic maps of northern Alaska, Harrison Bay quadrangle: U.S. Geological Survey Open-File Report 85-256, 47 p., scale 1:250:000.

Carter, D.L., and Galloway, J.P., 2005, Engineering geologic maps of northern Alaska, Harrison Bay quadrangle *with a section on* the digitally revised engineering geologic maps of northern Alaska, by D.W. Houseknecht, C.P. Garrity, and D.C. Meares: U.S. Geological Survey Open-File Report 2005-1194, 32 p., scale 1:250:000, available only online at http://pubs.usgs.gov/of/2005/1194/.

Clark, R.N., Swayze, G.A., Wise, Richard, Livo, K.E., Hoefen, T.M., Kokaly, R.F., and Sutley, S.J., 2003, USGS digital spectral library splib05a: U.S. Geological Survey Open-File Report 03-395, available only online at http://speclab.cr.usgs.gov/spectral-lib.html.

Crain, R.B., 1971, Preprocessing techniques to reduce atmospheric and sensor variability in multispectral scanner data, *in* Proceedings of the Seventh International Symposium on Remote Sensing of Environment, Ann Arbor: Environmental Research Institute of Michigan, p. 1345-1354.

Farrand, W.H., and Harsanyi, J.C., 1997, Mapping the distribution of mine tailings in the Coeur D'Alene River Valley, Idaho area through the use of a constrained energy minimization technique: Remote Sensing of Environment, v. 59, p. 64-76.

Garrity, C.P., 2004, Digital cartographic production techniques using airborne interferometric synthetic aperture radar (IFSAR) North Slope, Alaska, *in* Soller, D.R., ed., Digital Mapping Techniques '04—Workshop Proceedings: U.S. Geological Survey Open-File Report 2004-1451, p. 47–52.

Harsanyi, J.C., and Chang, C., 1994, Hyperspectral image classification and dimensionality reduction—An orthogonal subspace projection approach: IEEE Transactions on Geoscience and Remote Sensing, v. 32, p. 770-785.

National Oceanic and Atmospheric Administration, 2005, Precipitation data tables; Ashville, N.C., National Climate Data Center, available only online at http://www.ncdc.noaa.gov/oa/climate/online/ccd/nrmpcp.txt.

Research Systems Incorporated, 2000, 3.4 ENVI users guide: Boulder, Colo., Research Systems Inc., 864 p.